## Thiospinels

# Straightforward High-Pressure Synthesis and Characterization of Indium-Based Thiospinels: Photocatalytic Potential for Hydrogen Production

Horacio Falcón,[a,b] Pedro Tartaj,[a] Fernando Vaquero,[c] Rufino M. Navarro,[c]
Jose Luis G. Fierro,[c] Juan P. Bolletta,[d] Juan M. de Paoli,[d][‡] Raul E. Carbonio,[d][‡]
Maria Teresa Fernández-Díaz,[e] and Jose Antonio Alonso*[a]

**Abstract:** Ternary chalcogenides ($AB_2X_4$) based on the spinel structure are gaining a great deal of attention because of the possibility of tuning their magnetic and optoelectronic properties not only by changing chemical composition but also by altering their degree of inversion. Here we report a rapid high-pressure synthetic method for the synthesis of $MIn_2S_4$ powders starting from commercially available solid sulfides. We prove the versatility of our method by reporting the synthesis of six members of the $MIn_2S_4$ family (M = Mn, Fe, Co, Ni, Zn, and Cd) under high-pressure conditions (3.5 GPa); these compounds show complete to moderate degrees of inversion. Furthermore, this family covers a spectral region that includes visible band gaps. Interestingly, the structural refinement carried out by X-ray and neutron diffraction allows one to establish positive correlations between the gap and different parameters, including the degree of inversion. Finally, as a proof-of-concept, these ternary chalcogenides show moderate photocatalytic hydrogen production from aqueous solutions.

## Introduction

Most $AB_2S_4$ thiospinels are semiconductors with $S^{2-}$ ions arranged in a close-packed fcc structure defined by the space group $Fd\bar{3}m$. They contain A cations tetrahedrally coordinated by sulfide anions, and B ions at octahedral sites. Since the pioneering work by Goodenough on indium thiospinels $MIn_2S_4$ (M = Mn, Fe, Co, and Ni),[1] in which the author explained the different magnetic interactions that depended on the degree of inversion of cations between A and B sites, these materials have attracted the interest of solid-state scientists. The possibility of tuning their magnetic and optoelectronic properties not only by changing the chemical composition but also by altering the degree of inversion has significantly renewed the broader interest in thiospinels. Specifically, some thiospinels are being explored as active materials that exhibit both ferromagnetic and semiconducting properties,[2,3] whereas others show photoluminescence[4] and have found applications as photoconverters.[5]

Recently these materials were described to have potential use in solar-driven applications. Some thiospinels with band gaps in the visible range are being used in photovoltaic devices and for photocatalytic degradation of colorants. Thiospinels are also being explored as photocatalysts for hydrogen production under visible-light irradiation.[6–20] Water splitting from solar energy mediated by semiconductor catalysts with a band gap within the visible part of the spectrum is theoretically the most efficient process for conversion of solar energy into hydrogen.[10,21,22] In indium-based thiospinels in particular, band-gap tuning is possible both by altering the chemical composition and the degree of spinel inversion.[1,9,23–25] The combination of these two effects in thiospinels is expected to be a powerful tool to obtain materials with adequate characteristics for photocatalytic activity within the solar spectrum.

Among the different methods to synthesize indium thiospinels described in the literature, those that involve conventional solid-state reactions require long thermal treatments in sealed quartz ampoules or under a strong sulfidizing atmosphere ($H_2S$), whereas those that involve liquid precursors usually require the use of organic additives and often expensive precursors.[15,26–33] Thus, there is interest in implementing new methodologies that are able to produce, within relatively short reaction times, thiospinels by starting from easily available commercial solid precursors. Furthermore, it would be desirable to obtain these spinels in the absence of any organic additives that could alter the properties of the materials. The active surface

[a] Instituto de Ciencia de Materiales de Madrid, CSIC,
Cantoblanco, 28049 Madrid, Spain
E-mail: ja.alonso@icmm.csic.es
http://www.icmm.csic.es/matfuelcells/
[b] NANOTEC (Centro de Investigación en Nanociencia y Nanotecnología),
Universidad Tecnológica Nacional-Facultad Regional Córdoba,
Córdoba, Argentina
[c] Instituto de Catálisis y Petroleoquímica, CSIC,
Cantoblanco, 28049 Madrid, Spain
[d] INFIQC - CONICET, Departamento de Fisicoquímica, Facultad de Ciencias
Químicas, Universidad Nacional de Córdoba
Haya de la Torre esq. Medina Allende, X5000HUA Córdoba, Argentina
[e] Institut Laue Langevin,
BP 156X, 38042, Grenoble, France
[‡] Members of the Research Career of CONICET
Supporting information and ORCID(s) from the author(s) for this article are
available on the WWW under http://dx.doi.org/10.1002/ejic.201501390.

ChemPubSoc
Europe

EurJIC
European Journal
of Inorganic Chemistry

Full Paper

where the photocatalytic reactions take place is especially sensitive to the presence of organic moieties.[34]

In this paper we describe the preparation of six thiospinels, $MIn_2S_4$ (M = Mn, Fe, Co, Ni, Zn, Cd), by means of an alternative yet straightforward procedure that involves the thermal treatment under high pressure of mixtures of simple sulfides for reaction short times, typically 1 h, that yield pure specimens (in most cases) with good crystallinity and attractive physical properties. Selection of these six thiospinels was based on three criteria: (i) Band-gap tunability, as this family includes elements with different electronegativity,[35] differences in covalent mixing between anionic and cationic orbitals,[25] 3d electrons more or less localized with orbitals half or fully filled,[36] and elements that are known to show peculiar behavior in B sites;[1] (ii) earth-abundant elements (especially Fe, Mn, and Ni); and (iii) the existence of previous studies that showed the viability of photocatalytic hydrogen production under visible irradiation ($ZnIn_2S_4$ and $ZnIn_2S_4/CdIn_2S_4$ heterostructures).[10,15,16,37] These materials were characterized by XRD and neutron powder diffraction to determine their crystallographic features, such as the degree of inversion. As a proof-of-concept of our synthesis route, the ternary thiospinels that exhibited visible gaps from 2.6 to 1.9 eV show photoactivity for hydrogen evolution from aqueous solutions under visible light.

The synthesis qualifies as "straightforward" with respect to the standard methods of preparation of thiospinels that involve long thermal treatments (multiple days, multiple times) under $H_2S$ currents and often yield mixtures of several phases. The synthesis conditions can be easily reached in a modest piston-cylinder press, which is present in many solid-state chemistry laboratories. Additionally, identical experimental conditions (temperature, pressure, time) were utilized to prepare six different thiospinels that include cations of diverse chemical nature in their composition. It is also worth noting that some of the spinels described here (for instance, $NiIn_2S_4$) could not be prepared by conventional methods (solid-state reactions under ambient pressure and $H_2S$ flow).

## Results and Discussion

### Structural Characterization

Samples with nominal stoichiometries of $MIn_2S_4$ (M = Mn, Fe, Co, Ni, Zn, and Cd) were obtained as well-crystallized powders after the high-pressure treatments. No reaction with Pt from the container capsule was ever detected. The samples were compact pellets that were ground for characterization. The XRD diagrams are shown in Figure 1a–e along with their respective Rietveld refinements, as indicated below. The patterns are characteristic of single-phase spinel sulfides and they can all be indexed in a cubic unit cell in the space group $Fd\bar{3}m$ (except for M = Zn), with the unit-cell parameters varying between $a$ = 10.4959(2) Å for M = Ni and $a$ = 10.8321(3) Å for M = Cd, as indicated in Table 1. For M = Zn the sulfide adopts its own structural type ($ZnIn_2S_4$ type), defined by the rhombohedral $R\bar{3}m$ space group, with $a$ = 3.8722(1) Å and $c$ = 37.0397(8) Å. This compound is not a canonical spinel; it does not adopt the
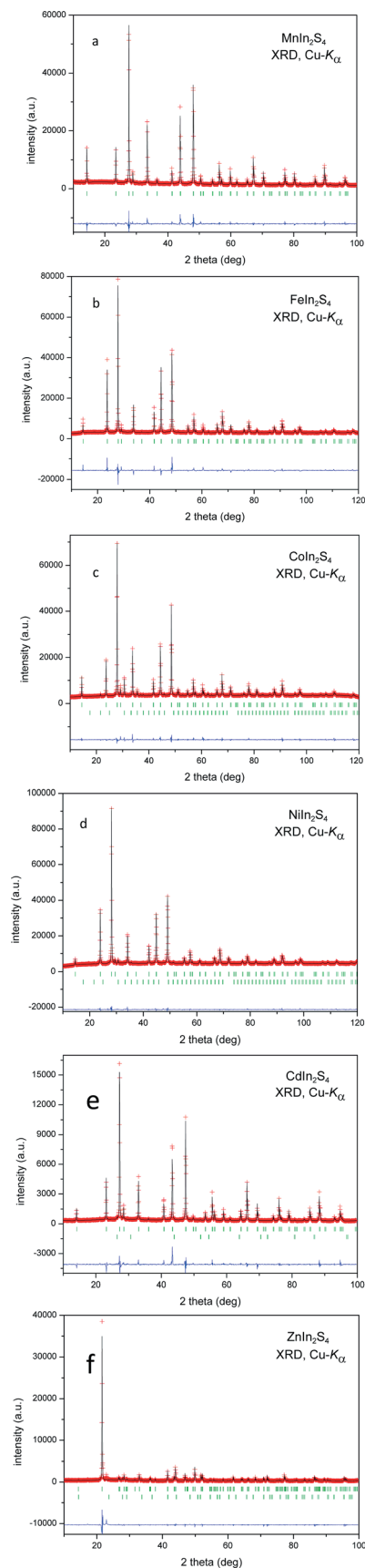


Figure 1. XRD patterns of $MIn_2S_4$ after the Rietveld refinement in a face-centered cubic unit cell, $Fd\bar{3}m$ space group (M = Mn, Fe, Co, Ni, Cd), or $ZnIn_2S_4$ type, $R\bar{3}m$ space group. The second series of Bragg reflections (vertical markers) corresponds to minor amounts of $In_2S_3$ (M = Co, Ni), CdS (M = Cd), and cubic $ZnIn_2S_4$ spinel (M = Zn).

ChemPubSoc
Europe

EurJIC
European Journal
of Inorganic Chemistry

Full Paper

Table 1. Unit-cell, positional, displacement B parameters, site occupancies, and main interatomic distances and valences for $MIn_2S_4$, refined in the cubic $Fd\bar{3}m$ space group (no. 227), origin at center ($\bar{3}m$), from XRD data at 295 K. Tetrahedral and octahedral positions are $8a$ (1/8,1/8,1/8) and $16d$ (1/2,1/2,1/2) crystallographic Wyckoff sites, respectively; $S^{2-}$ ions locate at $32e$ ($u,u,u$). Bond lengths are given in Å. $\lambda$ is the inversion degree of the spinel structure.

| M | Mn | Fe | Co | Ni | Cd |
|---|---|---|---|---|---|
| $a$ [Å] | 10.7251(4) | 10.6020(3) | 10.6049(2) | 10.4959(2) | 10.8321(3) |
| $u$(S) | 0.2548(3) | 0.2621(3) | 0.2573(2) | 0.2588(2) | 0.2544(4) |
| $f_{occ}$M/In ($8a$) | 0.540/0.460 | 0.059/0.941 | 0.391/0.609 | 0.096/0.904 | – |
| $f_{occ}$M/In ($16d$) | 0.230/0.770 | 0.470/0.530 | 0.305/0.695 | 0.451/0.549 | – |
| $\lambda$ | 0.460(4) | 0.941(4) | 0.609(5) | 0.904(5) | – |
| (M–S)$_{tetra}$ (×4) | 2.410(3) | 2.518(3) | 2.430(2) | 2.422(2) | 2.428(4) |
| (In–S)$_{octa}$ (×6) | 2.632(3) | 2.529(3) | 2.576(2) | 2.535(2) | 2.661(4) |

cubic structure but a rhombohedral superstructure with much larger unit-cell parameters.[38] In accordance with this, SEM micrographs (Figure 2) show a very distinct morphology for $ZnIn_2S_4$ (platelets) and the as-synthesized cubic spinels, which are shaped like truncated octahedra. The differences in sizes are probably due to the specifics of the diffusion reaction and/or to the nature of the commercial solid precursors.
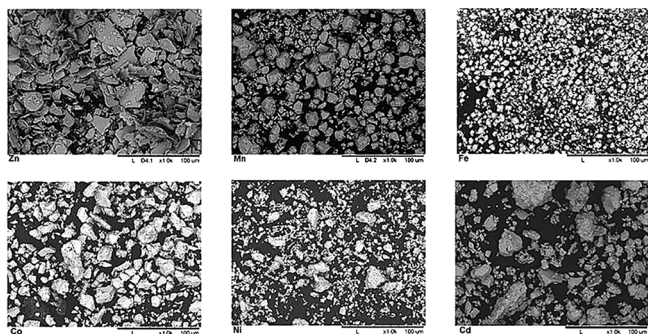


Figure 2. SEM micrographs of $MIn_2S_4$ samples (M = Zn, Mn, Fe, Co, Ni, Cd). The scale bar is the same in all pictures.

The refinement of the crystal structure of the cubic thiospinels $MIn_2S_4$ (M = Mn, Fe, Co, Ni, and Cd) was performed on the basis of laboratory XRD data obtained at room temperature with Cu-$K_\alpha$ radiation. Additionally two neutron diffraction patterns were collected for M = Fe, Mn. Although the absorbing nature of In only allowed the acquisition of poor statistical NPD data, they were found useful for the determination of the individual displacement B factors; the results of the NPD refinements are included in the Supporting Information (Tables S2 and S3 for Mn and Fe, respectively; Figures S1–S3).

The structure was defined in the cubic space group $Fd\bar{3}m$ (no. 227), origin at center ($\bar{3}m$). In a first approach, $M^{2+}$ and $In^{3+}$ cations were located at $8a$ (1/8,1/8,1/8) and $16d$ (1/2,1/2,1/2) crystallographic Wyckoff sites, respectively, and sulfide anions at $32e$ ($u,u,u$) positions. Antisite disordering considering that some M could occupy the octahedral $16d$ sites and some In the tetrahedral $8a$ positions was refined, whereby we observed a significant drop of the discrepancy of the $R_{Bragg}$ factor down to 5–7 %. This is related to the degree of inversion of each spinel. A further refinement of the occupancy factor of the sulfide anions led to a full stoichiometry of the anionic sublattice within the standard deviations. Excellent fits were obtained for this model, as shown in Figure 1. The most important structural parameters of the crystal structure at room temperature and

the discrepancy factors after the refinements are listed in Table 1, as well as the main interatomic distances in both tetrahedral and octahedral coordination units. A view of the crystal structure of $MIn_2S_4$ spinels is illustrated in Figure 3. In the $CoIn_2S_4$ XRD pattern, CoS was identified as minor impurity; it was introduced as a second phase in the refinement and quantified as 6.5(1) %.
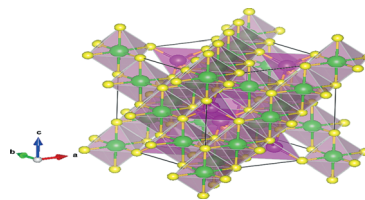


Figure 3. View of the crystal structure of $MIn_2S_4$ for an ideal (non-inverted) spinel with M at the tetrahedral voids and In at octahedral positions.

Regarding the Zn compound, the hugely preferred orientation observed in the XRD pattern prevented the full refinement of the crystal structure. This is supported by the observation of the platelet-like morphology in the SEM micrographs (Figure 2). However, it was possible to carry out a Le Bail fit by starting from the unit-cell parameters given in the literature for the rhombohedral cell defined by the $R\bar{3}m$ space group.[38] After the pattern matching we obtained $a$ = 3.8722(1) Å and $c$ = 37.0397(8) Å. A contribution of a cubic spinel of the same composition, $ZnIn_2S_4$, was found and introduced as a second phase in the refinement. In this case a unit-cell size of $a$ = 10.635(2) Å was refined for a normal spinel with Zn at the tetrahedral sites and In at the octahedral positions. The good agreement found between observed and calculated intensities is shown in Figure 1f.

In cubic $AB_2S_4$ thiospinels the cations at the special positions $8a$ (space group $Fd\bar{3}m$) show tetrahedral sulfur coordination, and those at $16d$ are in octahedral coordination, whereas the sulfur anions occupy the general positions $32e$. Only two parameters determine the structure of a spinel: the lattice constant $a$ and the anion parameter $u$. A classical problem is the determination of the ion distribution over the octahedral and tetrahedral sites. This distribution is conveniently characterized by specifying the inversion parameter ($\lambda$), which is defined as the fraction of B cations at tetrahedral sites. In an ideal spinel the anions form a cubic sublattice with $u$ = 0.25 [considering the origin at center ($\bar{3}m$)], but normally the anions are displaced along a [111] direction and the positional parameter $u$ must be specified.

ChemPubSoc
Europe

EurJIC
European Journal
of Inorganic Chemistry

Full Paper

In the present case, the degree of inversion could be determined from the refinement of the crystal structure of $MIn_2S_4$ (M = Mn, Fe, Co, Ni) from XRPD data; for M = Cd the similar scattering factors for $In^{3+}$ and $Cd^{2+}$ prevented its direct determination. The remaining thiospinels show a variable degree of inversion; if we define it as the proportion of In at tetrahedral sites, $\lambda$ is quite high for M = Ni and Fe (almost completely inverted spinels with $\lambda = 0.94$, 0.90 for Fe and Ni, respectively) and moderate for Co and Mn. They must therefore be considered as partially inverse spinels. Interestingly, the variable parameter for the $S^{2-}$ position, included in Table 1, is close to that expected for normal spinels ($u = 0.25$) for M = Mn and Co, and more elevated for Ni [$u = 0.2588(2)$] and Fe [$u = 0.2621(3)$]. Although the inversion degree for M = Cd could not be directly determined from the occupancy factors given the similar scattering of In versus Cd, its $u$ parameter [0.2544(4)] suggests that the degree of inversion is moderate.

As shown in Table 1, (M,In) ions at 8$a$ sites are fourfold coordinated within regular tetrahedral units. The (M,In)–S distances for the less inverted spinel M = Mn is 2.410(3) Å, which is in good agreement with the ionic-radii sum[39] for averaged $^{IV}Mn^{2+}$ (0.66 Å), $^{IV}In^{3+}$ (0.62 Å) cations, and $^{VI}S^{2-}$ (1.84 Å) of 2.48 Å. For the most inverted specimen, M = Fe, the ionic-radii sum of averaged $^{IV}Fe^{2+}$ (0.63 Å), $^{IV}In^{3+}$ cations, and $^{VI}S^{2-}$ of 2.42 Å is considerably shorter that the observed distance of 2.518(3) Å. In the octahedral units, (M,In)–S bond lengths vary between 2.529(3) Å (M = Fe) and 2.661(4) Å (M = Cd), which are comparable to the expected distance for In–S pairs. The longest distance observed for (Cd,In)$S_6$ octahedra agrees well with the fact that the inversion degree of Cd specimen is moderate, and hence, there is a large content of In at the octahedral position, whereas Cd preferentially occupies the tetrahedral voids. In the case of Zn, although the crystal structure could not be refined from the XRD pattern owing to a serious problem with preferred orientation (related to the layered rhombohedral structure and the morphology of the crystallites found for this compound, which adopts its own structural $ZnIn_2S_4$ type), we can compare the Zn–S and In–S distances provided elsewhere at the tetrahedral and octahedral sites of 2.378 and 2.621 Å, respectively.[38] The Zn–S bond lengths are the shortest among the tetrahedral distances observed in this series, whereas the In–S distances are similar to those observed for M = Mn and Cd, perhaps suggesting that the inversion degree of this spinel superstructure is also moderate.

Moreover, to gain insight into the actual valences of M and In ions at both coordination environments, the results of the calculation of the bond valences (Table 2) would be extremely interesting,[40–42] despite the intrinsic ionic disorder introduced by the inversion. In Brown's model,[40] the valence is the sum of the individual bond valences ($s_i$) for M–S and In–S bonds. Bond valences were calculated as $s_i = \exp[(r_0 - r_i)/B]$; $B = 0.37$, $r_0 = 2.37$ for the $In^{3+}$–$S^{2-}$ pair and $r_0 = 2.22, 2.12, 1.94, 1.98$, and 2.304 for the $M^{2+}$–$S^{2-}$ pairs (M = Mn, Fe, Co, Ni, Cd).[42] Individual M–S and In–S distances ($r_i$) at tetrahedral and octahedral positions are taken from Table 1. Several trends can be identified in Table 2: (i) The valences of In at the octahedral sites for the most inverted spinels (which contain roughly half of each

M and In ion) are much higher than the expected value of 3+, since the sites are shared with $M^{2+}$ ions with lower ionic radius. (ii) In is extremely overbonded in M = Fe, Ni, and even Co thiospinels. For the less inverted spinels (Mn and probably Cd), the In valence at $InS_6$ octahedra is closer to the expected value (i.e., +2.95 for Mn and +2.74 for Cd). Regarding the M–S bonds, the most inverted spinels show unrealistically low values (around +1) for Fe, Co, and Ni at $(In,M)S_4$ tetrahedra, since the occupancy is dominated by In. (iii) The valence is closer to the divalent value for Mn (+2.39), whereas for the Cd specimen the Cd valence is +2.86, which suggests that the bond is much shorter and the contribution of covalence is probably much higher in this second-row transition metal. Reasonable valences were obtained for Mn (+1.97) and Fe (+1.99) at $MS_6$ octahedra.

Table 2. Valences determined from the bond valence model for M and In in $MIn_2S_4$ at 295 K from XRD data.

| M | Mn | Fe | Co | Ni | Cd |
|---|---|---|---|---|---|
| Tetrahedral site | | | | | |
| M–S | 2.39(1) | 1.366(6) | 1.064(3) | 1.181(3) | 2.868(2) |
| In–S | 3.60(2) | 2.68(1) | 3.40(1) | 3.386(9) | |
| Octahedral site | | | | | |
| M–S | 1.97(7) | 1.988(7) | 1.075(3) | 1.337(3) | |
| In–S | 2.95(5) | 3.91(1) | 3.437(8) | 3.837(8) | 2.738(1) |

## Reflectance Measurements

Figure 4 shows the UV/Vis absorption spectra for all the $MIn_2S_4$ samples that cover compositions with visible band gaps. This shift in gaps can be qualitatively correlated with the structural data and the chemical composition of samples. Interestingly, the band gaps were observed to strongly depend on the degree of inversion. As already analyzed, the structural data point to two distinctive groups within the six-member family separated by the degree of inversion: (i) Mn, Zn, and Cd thiospinels that show a moderate degree of inversion, and (ii) Ni and Fe thiospinels that show an almost complete inversion. The thiospinels of group (i) with In mostly occupying the octahedral
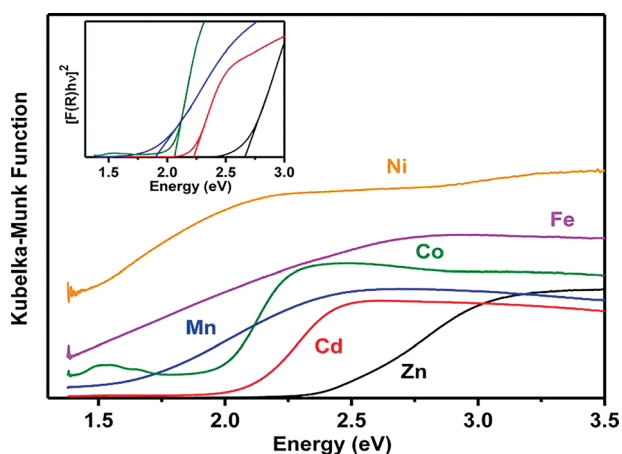


Figure 4. Kubelka–Munk absorbance spectra $F(R) = \alpha = (1 - R)^2/2R$ derived from diffuse reflectance data ($R$). (Inset) Absorption energy gaps for Zn (2.6 eV), Cd (2.2 eV), Co (2.1 eV), and Mn (1.9 eV) were obtained from Tauc plots assuming a direct transition.

ChemPubSoc
Europe

EurJIC
European Journal
of Inorganic Chemistry

Full Paper

positions present the higher absorption energy gaps. In the Co thiospinel, the inversion degree reaches an intermediate value, hence it was excluded from this analysis. In addition, Figure 4 shows low-intensity bands at around 750 and 810 nm for M = Co that suggest the existence of a portion of unreacted precursors, as indeed was detected by XRD.

Following the premise that correlations between gaps and differences in the structural data and chemical composition of samples must be carried out on the basis of a similar inversion degree, we first dealt with the group that shows moderate inversion (Mn, Zn, and Cd). In the group that shows moderate inversion (Mn, Zn, and Cd), we can differentiate between Mn and Cd/Zn thiospinels. Cd and Zn belong to the same group of the periodic table and have $d^{10}$ electron configurations. Interestingly, in $CdIn_2S_4$ there is no appreciable reduction in gap energies associated with the d orbitals, as they lie below the top of the valence band and hence do not mix.[23,25] Similar behavior is expected for $ZnIn_2S_4$. Therefore, differences in gaps between these two thiospinels should be sensitive to differences in electronegativity (assuming similar degrees of inversion). Furthermore, Cd and Zn have similar electronegativities (1.69 and 1.65 on the basis of Pauling electronegativity scale). Thus doping of the parent phase ($In_2S_3$) with any of these two elements is expected to lead to Cd and Zn thiospinels with a similar optical gap. In fact, $In_2S_3$ crystallizes in a defect spinel lattice that results in a tetragonal superstructure with ordered vacancies ($\beta$-$In_2S_3$) and a cubic structure ($\alpha$-$In_2S_3$) when cation sites and vacancies are randomly distributed.[43] The cation distribution of $In_2S_3$ may be written as $(In^A_{0.67}\square_{0.33})In^B_2S_4$, with $\square$ denoting unoccupied A sites. Both $\beta$- and $\alpha$-$In_2S_3$ structures have a band gap of approximately 2.1 eV. Doping of the parent phase with Cd leads to a $CdIn_2S_4$ thiospinel with a gap of 2.2 eV, whereas doping with Zn leads to a $ZnIn_2S_4$ thiospinel with a gap of 2.6 eV (Figure 4). Experimentally, we observe a shift of 0.4 eV (Figure 4). Recently, density functional calculations carried out for $CdIn_2S_4$ thiospinels have predicted a strong dependence of absorption energy gaps on the degree of inversion.[9] Shifts to lower energies of approximately 1 eV are estimated from a normal spinel to a spinel with an inversion degree of 0.5. Therefore, we understand that a difference of 0.4 eV in gaps between the Zn and Cd thiospinels is acceptable. This shift can be explained by slight differences in the inversion degree, and the fact that in the Zn thiospinel we have – in addition to the rhombohedral superstructure – a contribution from a cubic spinel.

For $MnIn_2S_4$, the other thiospinel with a moderate inversion degree, the structural data lead to a formula in which approximately 50 % of the $Mn^{2+}$ cations are positioned at tetrahedral and octahedral sites $[(In_{0.46}Mn_{0.54})^A(In_{1.54}Mn_{0.46})^BS_4]$. When compared to Cd/Zn thiospinels, arguments based on electronegativity [1.55 (Mn) versus 1.69 (Cd) and 1.65 (Zn) on the Pauling scale] and possible stabilization of the half-filled $3d^5$ ground state would suggest an increase in the band gap.[35,36] Experimentally, we observe a decrease to 1.9 eV versus 2.2–2.6 eV. There are two alternative/complementary scenarios: (i) As we are dealing with a half-filled configuration, the dependence of the band gap on the degree of inversion is significantly differ-

ent to that of Cd and Zn; and (ii) the cationic d orbitals mix with anionic orbitals (significant covalent mixing).

As mentioned above, in our six-member family, Ni and Fe thiospinels are characterized by an almost complete inverted structure (>90 % of $Ni^{2+}$ and $Fe^{2+}$ cations are positioned at octahedral sites; Table 1). The inferred gaps of these inverted thiospinels (Figure 4) are significantly shifted to lower energies relative to the parent phase ($In_2S_3$) and the spinels with moderate inversion (Mn, Zn, Cd). This result confirms that there is a strong dependence of absorption energy gaps on the inversion degree in thiospinels. A comparison between the absorption spectra of Ni and Fe is also interesting. From Figure 4 we also infer an optical gap of lower energy for the Ni thiospinel. Interestingly, the valences of In at the octahedral sites, where most of the Ni and Fe are positioned (Table 2), as already mentioned, are much higher than the expected value of +3 (+3.91 and +3.84 for In in Fe and Ni thiospinels, respectively). The valence derived from the structural data and bond valence models (Table 2) for Ni at octahedral positions leads to a value of +1.34. Basically, when replacing Ni with Fe cations, we can expect parameters such as electronegativity to influence the gap shift. Indeed, the electronegativity of Ni is higher than that of Fe (1.93 for Ni versus 1.81 for Fe on the Pauling scale), which would explain the shift to lower energy of the gap in the Ni thiospinel.

## Photocatalytic Activity

Water splitting into $H_2$ and $O_2$ is an uphill reaction and requires a free-energy change of 237 kJ $mol^{-1}$ (or 1.23 eV). For efficient production of $H_2$, the band gap of the photocatalysts must be between 3.0 eV (420 nm) and 1.23 eV (1000 nm).[10] In practical applications, photons above 1.5–1.7 eV or even higher (2.0 eV) are required owing to energy barriers (over potentials).[44] Moreover, the conduction-band (CB) and valence-band levels (VB) should meet the energy requirements set by the reduction of water (H + e− → 1/2 $H_2$ $E^0$ = 0.0 V) and the oxidation potential of $S^{2-}/SO_3^{2-}$ ($S^{2-}$ + $SO_3^{2-}$ + 2 h+ → $S_2O_3^{2-}$ $E^0$ = –0.72 V), respectively. According to the absorption spectra shown in Figure 4 and these lower limits, we have four compositions that could be suitable for hydrogen production ($MIn_2S_4$; M = Mn, Co, Cd, Zn). The composition that contains Co was excluded from the photocatalytic experiments as it showed some unreacted CoS (Figure 1c, and detailed analysis above). Interestingly, X-ray photoelectron spectroscopy analyses of the surfaces only showed the presence of S, In, and M atoms (Mn, Cd, or Zn) with a stoichiometry similar to that of bulk for the Mn and Cd thiospinels and slightly enriched in In atoms for the Zn thiospinel (Table S4 in the Supporting Information).

Photocatalytic hydrogen evolution over $MIn_2S_4$ (M = Zn, Cd, or Mn) samples was evaluated under visible-light irradiation using $Na_2S/Na_2SO_3$ as sacrificial reagents. Control photoactivity experiments were performed in the absence of light irradiation, catalysts, or sulfur sacrificial agents to corroborate if the activity of the samples is exclusively associated with these experimental variables. In all cases, the control experiments showed that no reaction occurred when the system was illuminated in the absence of catalyst or in the presence of catalyst without illumina-

ChemPubSoc
Europe

EurJIC
European Journal
of Inorganic Chemistry

Full Paper

tion or sulfur sacrificial electron-donor agents. Reactions that use sacrificial agents are considered half-reactions of water splitting. The use of sacrificial molecules as electron donors remarkably improves the $H_2$ production, as holes are scavenged by these molecules. Furthermore, the use of the $Na_2S/Na_2SO_3$ couple is expected to increase the stability against corrosion. For practical applications, the utilization of reactions that use sacrificial agents for $H_2$ fuel production will only be of interest if the agents are derived from biomass or from toxic residues. Even though, to the best of our knowledge, there are no thermodynamic data available to build Pourboix plots for the mixed thiospinels, the Pourboix plot of the parent phase ($In_2S_3$) is similar to CdS.[45] This similarity suggests that the Pourboix plot of the mixed thiospinels could be similar as well. Therefore, an additional role for the sacrificial agent would be to avoid the presence of free oxygen, as is required for other sulfide systems such as CdS.

The results for the photocatalytic hydrogen evolution over $MIn_2S_4$ (M = Zn, Cd or Mn) under visible-light irradiation using $Na_2S/Na_2SO_3$ as sacrificial reagents are shown in Figure 5. In the absence of Pt co-catalyst, the as-prepared $MIn_2S_4$ (Zn, Cd, Mn) samples show low $H_2$ production (Zn: 8.6 µmol h$^{-1}$ g$^{-1}$, AQE = 0.2 %; Cd: 3.9 µmol h$^{-1}$ g$^{-1}$, AQE = 0.1 %; Mn: 2.4 µmol h$^{-1}$ g$^{-1}$, AQE = 0.1 %). The $H_2$ production rate that corresponds to $ZnIn_2S_4$ = 8.6 µmol h$^{-1}$ g$^{-1}$ is small relative to reported values on fine particles of $ZnIn_2S_4$ (ca. 60 µmol h$^{-1}$ g$^{-1}$)[15] and is likely associated with the larger particles obtained through our synthetic route (Figure 2). The reason for the improvement in photocatalytic activity of the Zn thiospinel relative to Cd and Mn thiospinels is difficult to pinpoint, as it may be a contribution of different factors. $ZnIn_2S_4$ exhibits a different, layered, crystal structure, in contrast with the three-dimensional, conventional spinels observed for the other sulfides. The ease of exfoliation of the hexagonal $ZnIn_2S_4$ structure might offer a larger active area. Specific differences in the band structure and absorption of photons might also account for better efficiency in the Zn
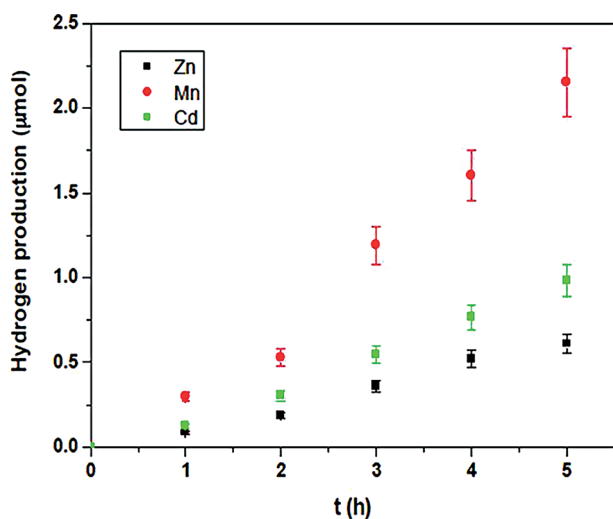
thiospinel. As mentioned below, even the slight differences in surface chemical composition detected by XPS (a stoichiometry similar to that of bulk for the Mn and Cd thiospinels and slightly enriched in In atoms for the Zn thiospinel) could account for this difference. Finally, crystallinity does not seem to play a significant role in improving efficiency, as all samples appear well crystallized.

To assess the stability of the three samples after the photocatalysis experiments, we recorded XRD patterns and XPS spectra. The XRD patterns (Figure S4 in the Supporting Information) correspond exactly to the same crystallographic spinel structure. There is no partial dissolution of the material or phase separation during the treatment. It seems that the materials are, at least kinetically, stable under the conditions of the photocatalysis experiments (i.e., pH temperature, illumination, presence of sacrificial agent). The relatively good stability of the sulfide phases was also evidenced by XPS of the three samples after the photocatalytic runs (Table S5 in the Supporting Information). All these samples displayed a rather narrow S 2p$_{3/2}$ component (FWHM = 1.6–1.7 eV) characteristic of S$^{2-}$ ions, which precludes the presence of other S species (e.g., disulfides, elemental sulfur). In addition, the O 1s level for these samples was recorded. In all cases a single O 1s component at a binding energy of 531.9–532.1 eV was measured. This rather high value corresponds to hydroxyl groups (OH) adsorbed on the sulfide phase.[46] As the oxidation of the S$^{2-}$ ions by these adsorbed OH$^-$ groups is an activated process, long reaction times are required at room temperature to start oxidation processes. For these three samples the binding energies of the cations of spinels remained virtually unchanged.

Finally, as mentioned above, we must keep in mind that the method here reported is intended for the stabilization of complex metal sulfides in only 1 h from commercial solid products, in the absence of organic additives and toxic flows ($H_2S$), and avoids the formation of stable metal oxides. When it comes to the identification of new photoactive compositions, the experimental observation of hydrogen production in $MnIn_2S_4$, which to the best of our knowledge has not been reported before, is certainly appealing. This thiospinel is very interesting because it shows a band gap of approximately 1.9 eV (red thiospinel) and Mn is an earth-abundant element.

## Conclusion

In this contribution we have shown that the facile synthesis of thiospinels by a straightforward high-pressure method from simple sulfides is possible. We have proven the versatility of our method by reporting the synthesis of six members of the $MIn_2S_4$ family (M = Mn, Fe, Co, Ni, Zn, and Cd) that display almost complete and moderate degrees of inversion. Furthermore, this family covers a spectral region that includes band gaps of interest in photocatalytic reactions under visible-light irradiation (from 2.6 to 1.9 eV). Interestingly, the structural refinements carried out by X-ray and neutron powder diffraction have allowed us to establish positive correlations between gaps and different parameters, including the degree of inversion. Therefore, any band-structure calculation or experimental com-



Figure 5. Hydrogen production from aqueous solutions containing $Na_2S$ + $Na_2SO_3$ sacrificial reagents under visible-light irradiation over the Mn, Cd, and Zn thiospinels.

parison in band gaps among thiospinels of different natures and/or prepared by different methods, should be based on a good estimation of the inversion degree. Finally, as a proof-of-concept of our synthetic route to rapidly screen active compositions, we have shown the experimental realization of hydrogen production from aqueous solution under visible-light irradiation over different thiospinels, including a red one with a band gap of approximately 1.9 eV ($MnIn_2S_4$). These promising results could be enhanced in milled materials with superior surface areas.

## Experimental Section

**Materials:** All solid precursors were obtained from Strem Chemicals (>99 % purity)—except $In_2S_3$, which was obtained from Alfa Aesar (>99 %)—and were used without further purification.

**Synthesis Protocol:** Polycrystalline samples of $MIn_2S_4$ (M = Mn, Fe, Co, Ni, Zn, and Cd) were obtained in a single step by thermal treatments under high-pressure conditions. Intimate mixtures of stoichiometric amounts of analytical-grade MS and $In_2S_3$ were put into a Pt capsule (5 mm diameter, 10 mm length), sealed, and placed in a cylindrical graphite heater. The reaction was carried out in a piston-cylinder press (Rockland Research Co.) under a hydrostatic pressure of 3.5 GPa at 1073 K for 1 h. Then the materials were quenched to room temperature, and the pressure was subsequently released.

**Structural Characterization:** The initial characterization was carried out by means of X-ray powder diffraction (XRPD) with a Bruker-AXS D8 diffractometer (40 kV, 30 mA) controlled by DIFFRACT-plus software in Bragg–Brentano reflection geometry with Cu-$K_\alpha$ radiation ($\lambda$ = 1.5418 Å) at room temperature. Neutron powder diffraction (NPD) patterns for M = Mn, Fe were acquired at the high-resolution D2B diffractometer of the Institut Laue Langevin (ILL) in Grenoble (France). The samples, which weighed 0.8 g, were packed in a vanadium holder 6 mm in diameter. The patterns were collected at 295 K with a wavelength of 1.594 Å and a counting time of 2 h in the high-intensity mode. The XRD and NPD patterns were analyzed by the Rietveld method using the FULLPROF program.[47] The line shape of the diffraction peaks was generated by a pseudo-Voigt function, and the background refined to a fifth-degree polynomial. The coherent scattering lengths for Mn, Fe, In, and S were –3.73, 9.45, 4.065, 2.847 fm, respectively. In the final run the following parameters were refined: background coefficients, zero-point, half-width, pseudo-Voigt and asymmetry parameters for the peak shape, scale factor, position of the sulfide anions (u), occupancy factors for A and B cations, thermal isotropic factors for all the atoms, and unit-cell parameters.

**Microstructural Characterization:** Scanning electron microscopy (SEM) was carried out with a tabletop Hitachi TT1000 microscope.

**Surface Characterization:** Photoelectron spectra (XPS) were acquired with a VG Escalab 200R spectrometer equipped with a hemispherical electron analyzer and an Al-$K_{\alpha1}$ ($h\nu$ = 1486.6 eV) 120 Watt X-ray source. The powder samples were stuck onto small stainless steel holders and then placed on a sample rod, placed in a pretreatment chamber, and degassed at room temperature under $10^{-5}$ mbar residual pressure for 2 h prior to being transferred to the analysis chamber. Before the spectra were recorded, the sample was maintained in the analysis chamber under a residual pressure of approximately $4 \times 10^{-9}$ mbar for 2 h. Survey and high-resolution spectra were collected at 45° to the detector with pass energy resolutions of 200 and 20 eV, respectively. The linearity of the binding
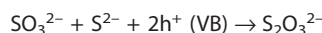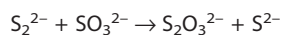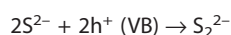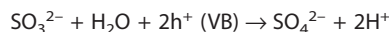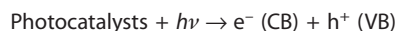
energy scale was calibrated against the Au 4$f_{7/2}$ (84.0 eV) and the Cu 2$p_{3/2}$ (932.6 eV) photoemission lines by standard procedures. Charge effects on the samples were corrected by referencing energies to the C 1s line at 284.8 eV. This reference gave BE values with an accuracy of ±0.2 eV. The high-resolution spectra for the regions of interest were curve-fitted using XPS Peak software. Curve fitting was performed using Gaussian–Lorentzian (90 %G–10 %L) shapes with a Shirley background. Atomic ratios were computed from the intensity ratios normalized by atomic sensitivity factors.[48]

**Reflectance Measurements:** Diffuse reflectance measurements were carried out with a UV/Vis spectrophotometer (Perkin–Elmer Lambda 35) equipped with a P/N AA-00214-100 integrating sphere reflectance unit (Spectralon LABSPHERE). The reflectance data ($R$) were converted into the Kubelka–Munk function: $F(R) = \alpha = (1 - R)^2/2R$. The optical band gap of samples was evaluated from the absorption spectrum using the Tauc relation[49] and assuming a direct allowed band gap [Equation (1)]:
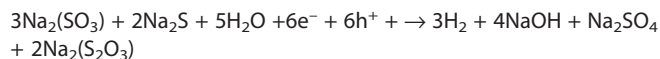
$$(\alpha h\nu) = C(h\nu - E_g)^n \tag{1}$$

in which $C$ is a constant, $\alpha$ is the molar absorption coefficient, $E_g$ is the average band gap of the material, and $n$ depends on the type of transition ($n = 1/2$ for direct transitions). The average band gap was estimated from the intercept on the $h\nu$ axis of the linear portion of the $(\varepsilon h\nu)^{1/n}$ versus $h\nu$ plots.

**Photocatalytic Activity:** The hydrogen evolution on polycrystalline samples of $MIn_2S_4$ (M = Zn, Cd, and Mn) was evaluated in a closed Pyrex glass reactor (250 mL total volume, 8 cm diameter) working at room temperature and under an Ar atmosphere. The photocatalyst powders (0.05 g) were dispersed by magnetic stirring in an aqueous solution (150 mL) that contained 0.05 M $Na_2S$ and 0.02 M $Na_2SO_3$ as sacrificial electron-donor agents.[50] Solution pH was 12.5. Using this mixed solution, the photocatalytic reaction should proceed as follows:[51]

Photocatalysts + $h\nu$ → e$^-$ (CB) + h$^+$ (VB)

$2H_2O$ + 2e– (CB) → $H_2$ + 2OH$^-$

$SO_3^{2-}$ + $H_2O$ + 2h$^+$ (VB) → $SO_4^{2-}$ + 2H$^+$

$2S^{2-}$ + 2h$^+$ (VB) → $S_2^{2-}$

$S_2^{2-}$ + $SO_3^{2-}$ → $S_2O_3^{2-}$ + $S^{2-}$

$SO_3^{2-}$ + $S^{2-}$ + 2h$^+$ (VB) → $S_2O_3^{2-}$

with the overall reaction being:

$3Na_2(SO_3)$ + $2Na_2S$ + $5H_2O$ +6e$^-$ + 6h$^+$ + → $3H_2$ + 4NaOH + $Na_2SO_4$ + $2Na_2(S_2O_3)$

In the previous mechanism, the oxidation of $S^{2-}$ can occur through one-electron oxidation with the formation of radical anion S$^-$*, which could spontaneously react by dimerization ($2S^{-*}$ → $S_2^{2-}$) to form the $S_2^{2-}$ species as proposed in the work of Steudel.[52] Nevertheless, the formation of disulfide dimers is strongly suppressed by the addition of $SO_3^{2-}$ ions because they are consumed according to the reaction: $S_2^{2-}$ + $SO_3^{2-}$ → $S_2O_3^{2-}$ + $S^{2-}$.

Before measurement, the solution was purged several times with Ar to ensure complete air removal. The reactor was irradiated at the top with white light from a Xe arc lamp (150 W, ozone free, LOT Oriel GmbH & CO KG). The light spot on the reactor was equal to the reactor area (50.3 cm$^2$). Optical irradiance impinging on the reactor was measured and is presented in Table S1 of the Supporting Information. Samples of the evolved gases were extracted periodically (every 1 h for a total reaction time of 5 h) and analyzed by means of GC with a thermal conductivity detector (TCD; Varian

chromatograph, Model Star 3400 CX) equipped with 5Å molecular sieves using Ar as carrier gas. Error bands that show the typical deviations in hydrogen production were calculated based on an average of three different runs. The apparent quantum efficiency was calculated on the basis of [Equation (2)]:

$$AQE = d[\text{H}_2]/dt/d[h\nu]\text{inc}/dt \tag{2}$$

in which $d[\text{H}_2]/dt$ is the rate of hydrogen production and $d[h\nu]\text{inc}/dt$ is the total optical power impinging on the sample.

**Supporting Information** (see footnote on the first page of this article): Tables with structural data and experimental characterization; XPS and neutron diffraction patterns and crystal structures; and XPS and XRD patterns after the photocatalytic runs.

## Acknowledgments

[1] J. B. Goodenough, *J. Solid State Chem.* **1972**, *4*, 292–293.
[2] A. Krimmel, Z. Seidov, G. G. Guseinov, A. I. Najafov, H. K. Von Nidda, A. Loidl, D. M. Többens, *J. Phys. Condens. Matter* **2005**, *17*, 3611–3618.
[3] S. V. Trukhanov, I. Bodnar, M. A. Zhafar, *J. Magn. Magn. Mater.* **2015**, *379*, 22–27.
[4] S. Ge, Z. Shui, Z. Zheng, L. Zhang, *Opt. Mater.* **2011**, *33*, 1174–1178.
[5] I. V. Bodnar, S. A. Pavlyukovets, V. Y. Rud, Y. V. Rud, *Semiconductors* **2009**, *43*, 1510–1513.
[6] S. Peng, S. G. Mhaisalkar, S. Ramakrishna, *Mater. Lett.* **2012**, *79*, 216–218.
[7] J. Mu, Q. Wei, P. Yao, X. Zhao, S.-Z. Kang, X. Li, *J. Alloys Compd.* **2012**, *513*, 506–509.
[8] X. Fu, X. Wang, Z. Chen, Z. Zhang, Z. Li, D. Y. C. Leung, L. Wu, X. Fu, *Appl. Catal. B* **2010**, *95*, 393–399.
[9] Y. Seminovski, P. Palacios, P. Wahnón, R. Grau-Crespo, *Appl. Phys. Lett.* **2012**, *100*, 102112.
[10] X. Chen, S. Shen, L. Guo, S. S. Mao, *Chem. Rev.* **2010**, *110*, 6503–6570.
[11] J. Ding, S. Sun, W. Yan, J. Bao, C. Gao, *Int. J. Hydrogen Energy* **2013**, *38*, 13153–13158.
[12] J. Ding, W. Yan, S. Sun, J. Bao, C. Gao, *ACS Appl. Mater. Interfaces* **2014**, *6*, 12877–12884.
[13] S. K. Apte, S. N. Garaje, R. D. Bolade, J. D. Ambekar, M. V. Kulkarni, S. D. Naik, S. W. Gosavi, J. O. Baeg, B. B. Kale, *J. Mater. Chem.* **2010**, *20*, 6095.
[14] P. Palacios, I. Aguilera, K. Sánchez, J. C. Conesa, P. Wahnón, *Phys. Rev. Lett.* **2008**, *101*, 046403.
[15] Z. Lei, W. You, M. Liu, G. Zhou, T. Takata, M. Hara, K. Domen, C. Li, *Chem. Commun.* **2003**, 2142–2143.
[16] S. Shen, L. Zhao, L. Guo, *Mater. Res. Bull.* **2009**, *44*, 100–105.
[17] L. Ye, Z. Li, *Appl. Catal. B* **2014**, *160–161*, 552–557.
[18] L. Wei, Y. Chen, J. Zhao, Z. Li, *Beilstein J. Nanotechnol.* **2013**, *4*, 949–955.
[19] S. Shen, P. Guo, L. Zhao, Y. Du, L. Guo, *J. Solid State Chem.* **2011**, *184*, 2250–2256.
[20] S. Shen, L. Zhao, L. Guo, *Int. J. Hydrogen Energy* **2010**, *35*, 10148–10154.
[21] R. M. Navarro Yerga, M. C. Álvarez-Galván, F. del Valle, J. A. Villoria de la Mano, J. L. G. Fierro, *ChemSusChem* **2009**, *2*, 471–485.
[22] D. R. Gamelin, *Nat. Chem.* **2012**, *4*, 965–967.
[23] W. Rehwald, *Phys. Rev.* **1967**, *155*, 861–868.
[24] F. J. Manjón, A. Segura, M. Amboage, J. Pellicer-Porres, J. F. Sánchez-Royo, J. P. Itié, A. M. Flank, P. Lagarde, A. Polian, V. V. Ursaki, I. M. Tiginyanu, *Phys. Status Solidi B* **2007**, *244*, 229–233.
[25] J. B. Goodenough, *J. Phys. Chem. Solids* **1969**, *6*, 261–280.
[26] F. Fang, L. Chen, Y. Chen, L. Wu, *J. Phys. Chem. C* **2010**, *114*, 2393–2397.
[27] S. S. Werner, A. Wold, *J. Solid State Chem.* **1972**, *4*, 286–291.
[28] S. Lei, K. Tang, Z. Fang, Y. Qi, H. Zheng, *Mater. Res. Bull.* **2006**, *41*, 2325–2333.
[29] X. Chen, Z. Zhang, X. Zhang, J. Liu, Y. Qian, *J. Cryst. Growth* **2005**, *277*, 524–528.
[30] S. Shen, L. Zhao, L. Guo, *J. Phys. Chem. Solids* **2008**, *69*, 2426–2432.
[31] X. Gou, F. Cheng, Y. Shi, L. Zhang, S. Peng, J. Chen, P. Shen, *J. Am. Chem. Soc.* **2006**, *128*, 7222–7229.
[32] B. Chai, T. Peng, P. Zeng, X. Zhang, X. Liu, *J. Phys. Chem. C* **2011**, *115*, 6149–6155.
[33] L. Brossard, L. Goldstein, M. Guittard, *Le J. de Physique Colloques* **1976**, *37*, C6-C493–C6-C495.
[34] T. Hisatomi, J. Kubota, K. Domen, *Chem. Soc. Rev.* **2014**, *43*, 7520–7535.
[35] J. Zaanen, G. A. Sawatzky, J. W. Allen, *Phys. Rev. Lett.* **1985**, *55*, 418–421.
[36] J. Zaanen, G. A. Sawatzky, *J. Solid State Chem.* **1990**, *88*, 8–27.
[37] Y. Yu, G. Chen, G. Wang, Z. Lu, *Int. J. Hydrogen Energy* **2013**, *38*, 1278–1285.
[38] S. A. Lopez-Rivera, A. J. Mora, D. Acosta Najarro, A. V. Rivera, R. Avila Godoy, *Semicond. Sci. Technol.* **2001**, *16*, 367–271.
[39] R. D. Shannon, *Acta Crystallogr., Sect. A* **1976**, *32*, 751–767.
[40] I. D. Brown, in: *Structure and Bonding in Crystals*, vol. 2 (Eds.: M. O'Keefe, A. Navrosky), **1981**, p. 1.
[41] N. E. Brese, M. O'Keeffe, *Acta Crystallogr., Sect. B Struct. Sci.* **1991**, *47*, 192–197.
[42] I. D. Brown, *Z. Kristallogr.* **1992**, *199*, 255–272.
[43] K. Kambas, J. Spyridelis, M. Balkanski, *Phys. Status Solidi* **1981**, *105*, 291–296.
[44] J. Liu, Y. Liu, N. Liu, Y. Han, X. Zhang, H. Huang, Y. Lifshitz, S.-T. Lee, J. Zhong, Z. Kang, *Science* **2015**, *347*, 970–974.
[45] D. D. Wagman, W. H. Evans, V. B. Parker, R. H. Schumm, I. Halow, S. M. Bailey, K. L. Churney, R. L. Nuttal, *J. Phys. Chem.* **1982**, *11*, 1–390.
[46] Y. Tanaka, H. Saito, Y. Tsutsumi, H. Doi, H. Imai, T. Hanawa, *Mater. Trans.* **2008**, *49*, 805–811.
[47] J. Rodríguez-Carvajal, *Phys. B* **1993**, *192*, 55–69.
[48] D. Briggs, M. P. Seah, *Practical Surface Analysis by Auger and X-ray Photoelectron Spectroscopy*, Wiley, Chichester, UK, **1990**.
[49] J. Tauc, R. Grigorovici, A. Vancu, *Phys. Status Solidi* **1966**, *15*, 627–637.
[50] I. Tsuji, H. Kato, H. Kobayashi, A. Kudo, *J. Am. Chem. Soc.* **2004**, *126*, 13406–13413.
[51] J. F. Reber, K. Meier, *J. Phys. Chem.* **1984**, *88*, 5903–5913.
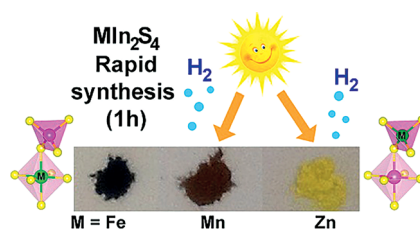[52] R. Steudel, *Ind. Eng. Chem. Res.* **1996**, *35*, 1417–1423.

■ **Thiospinels**

H. Falcón, P. Tartaj, F. Vaquero,
R. M. Navarro, J. L. G. Fierro,
J. P. Bolletta, J. M. de Paoli,
R. E. Carbonio,
M. T. Fernández-Díaz,
J. A. Alonso* ...................................... 1–9

**Straightforward High-Pressure Synthesis and Characterization of Indium-Based Thiospinels: Photocatalytic Potential for Hydrogen Production**

We describe a high-pressure synthetic method for $MIn_2S_4$ powders starting from commercially available solid sulfides (M = Mn, Fe, Co, Ni, Zn, and Cd) that show variable inversion degrees. This family covers a spectral region that includes visible band gaps. As a proof-of-concept, these ternary chalcogenides show moderate photocatalytic hydrogen production from aqueous solutions.